

# Fabrication and evaluation of photonic metamaterial crystal

S. Tanabete · Y. Nakagawa · T. Okamoto ·  
M. Haraguchi · T. Isu · G. Shinomiya

Received: 7 May 2013 / Accepted: 11 May 2013 / Published online: 1 June 2013  
© The Author(s) 2013. This article is published with open access at Springerlink.com

**Abstract** Many researching efforts have been reported to seek various fundamental LC resonance structures, recently. But still the Split Ring Resonator (SRR) is the most famous and major fundamental LC-resonance structure used in the metamaterial. We employed SRR structure as the fundamental LC-resonance mechanism to fabricate photonic crystal with periodic arrangement of two different metamaterial areas composed from SRR arrays on the dielectric substrate. We developed Photonic Metamaterial Crystal (PMC) to realize the more advanced and versatile functions of the metamaterial by 1 dimensional or 2 dimensional periodic arranging of two metamaterial sections which have different dispersion properties due to the different size of SRR structures each other. In this paper, we report the fabrication process, estimation of PMC properties and some possible future application prospects, for instance the PMC waveguide structures and nonlinear properties of PMC observed as selective LC-resonant properties in Raman mapping analysis of PMC. These are quite interesting charac-

ters of PMC and the attractive applications as the PMC devices.

## 1 Introduction

The metamaterial, which has the negative refractive index [1–3], is composed by LC resonance structure elements and background dielectric material [4–7]. We used typical SRR as the LC-resonance elements and arranged them in 2 dimensional square lattices or rectangular one to construct metamaterial which has a fundamental resonance frequency in near-infrared optical frequency and higher order resonance frequency in visible one. In general, the negative index band width which is realized by the SRR of LC-resonance dispersion is not so broad [8]. We attempted to utilize such a relatively narrow negative index band in SRR-based metamaterial to design its specific dispersion properties. We arrange the two kinds of SRR-based metamaterial sections, alternatively in certain periods whose resonance dispersion properties are different from each other. This structure may be possible to say a Photonic Metamaterial Crystal (PMC) [9]. We report such PMC fabrication process, properties and some possible applications.

## 2 Theoretical

### 2.1 Analytical model estimation of LC-resonance properties of SRR

The resonance frequency of a SRR structure which is shown in Fig. 1 can be estimated by the following analytical formula (1) as proposed by S. Tretyakov [10]:

---

S. Tanabete (✉) · T. Okamoto · M. Haraguchi  
Dept. of Optical Science and Technology, The University  
of Tokushima, Tokushima, Japan  
e-mail: [tanabe@opt.tokushima-u.ac.jp](mailto:tanabe@opt.tokushima-u.ac.jp)  
Fax: +81-88-6569411

M. Haraguchi (✉)  
e-mail: [haraguti@opt.tokushima-u.ac.jp](mailto:haraguti@opt.tokushima-u.ac.jp)  
url: [haraguti@opt.tokushima-u.ac.jp](http://haraguti@opt.tokushima-u.ac.jp)

T. Isu  
FRC, The University of Tokushima, Tokushima, Japan

Y. Nakagawa · G. Shinomiya  
Nichia Corp., Tokushima, Japan

$$\omega_0 = \frac{1}{\sqrt{(\varepsilon_r + (\pi/2)(L/g))(\mu_0\varepsilon_0(wh/2\pi)\ln(8L/(w+h)) + (1/\omega_p^2))}} \quad (1)$$

where the parameters in (1), i.e.  $w$ ,  $h$ ,  $t$  and etc., are defined in Fig. 1. The plasma frequency of gold is assumed to be equal  $\omega_p = 13.8 \times 10^{15} \text{ s}^{-1}$  and  $\varepsilon_r = 1$ . By using this formula to estimate SRR resonance frequency for the scaling, we obtained the results as shown in Fig. 2. The resonance frequency is increasing for the SRR physical size become smaller in same design as well known [11]. The material dispersion was taken account to correct this scaling curve. For example, we use metallic layer as the conductive material to make SRR structure. The metallic layer's properties, such as conductivity, dielectric constants and so on, change dramatically for the layer thickness as is well known [12, 13]. Thus, we evaluate the metallic layer properties by the attenuate total reflection (ATR) measurement in Kretschmann configuration [14].

To estimate the dielectric properties of the metallic layer, we used the theoretical reflectivity spectra to fit to the surface plasmon polariton (SPP) resonance damping dips in the angular scanning reflectance spectra obtained by ATR measurement in Kretschmann configuration. Also the conductance;  $\sigma$  of the metallic layer was derived by applying Drude model [15]. The obtained properties of the metallic layer were used for the calculation of LC-resonance proper-

**Fig. 1** SRR model structure with definitions of the geometrical parameters  $L = 200 \text{ nm}$ ,  $w = 50 \text{ nm}$ ,  $g = 100 \text{ nm}$ ,  $t = 120 \text{ nm}$ ,  $h$  (metal film thickness) =  $30 \text{ nm}$

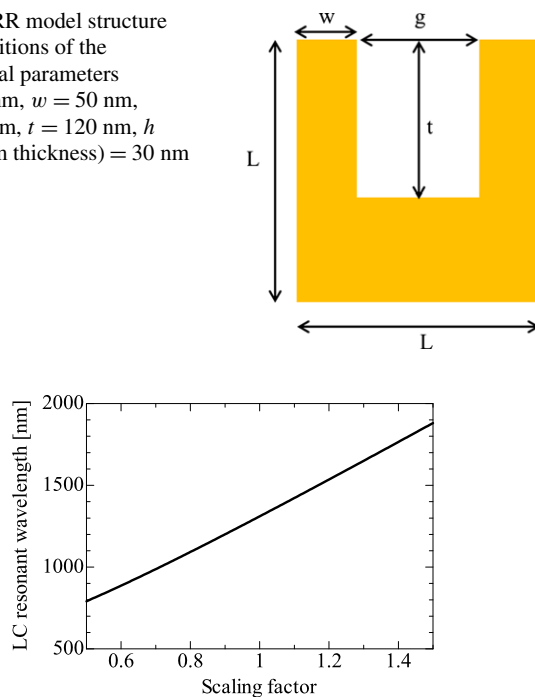


**Fig. 2** Resonance frequency for the SRR size

ties of the SRR structure. The theoretical formula of the ATR spectra is for the three layers model composed of a prism as a substrate, a metallic layer and air.

## 2.2 FDTD estimation of the SRR resonance properties

FDTD method is one of the most powerful tools to estimate the SRR resonance properties or the metamaterial properties numerically. The SRR on dielectric substrate was modeled as shown in Fig. 3. The other conditions used in calculation are listed in Fig. 3 and Figs. 4(a), (b). Figure 4 shows the electric field enhancement caused by the LC resonance at the mid gap position in a SRR as marked red solid circle in Fig. 3 obtained by FDTD simulation based on the SRR model in Fig. 3. The result in Fig. 4(a) is for the SRR made by gold (Au) layer and (b) is for one mode by silver (Ag) layer, respectively.

The SRR arrayed structure in a square lattice or rectangular one can be estimated by FDTD simulation as well known [8]. We are also developing the FDTD simulation for the PMC structures, but in this report's main role is a proposal of PMC and its application, thus we do not mention further the FDTD simulations.

## 3 Experimental

### 3.1 PMC fabrication

We summarize the fabrication process of the PMC structure based of SRR array as the dispersive elements. The

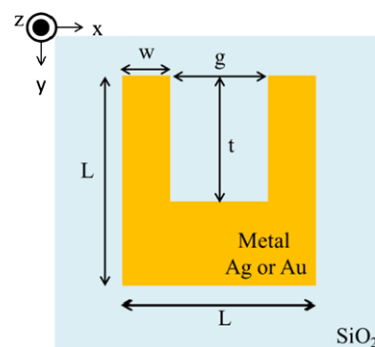


**Fig. 3** SRR model for the LC resonance simulation by FDTD method with definitions of simulations parameters  $L = 200 \text{ nm}$ ,  $w = 50 \text{ nm}$ ,  $g = 100 \text{ nm}$ ,  $t = 120 \text{ nm}$ ,  $h$  (metal film thickness) =  $30 \text{ nm}$ . These parameters are referenced, the resonance wavelength was calculated by scaling

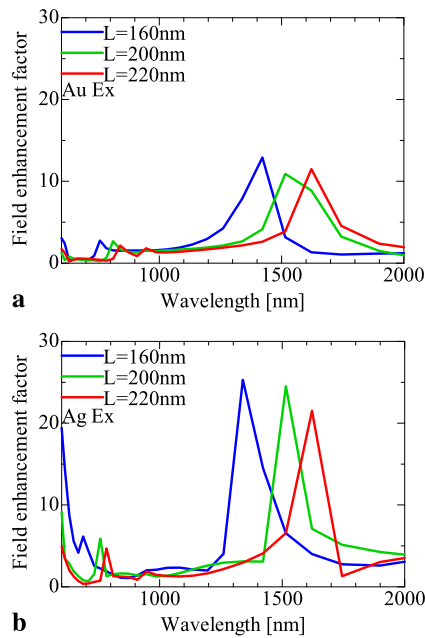


**Fig. 4** Estimated field intensity enhancement by LC resonance of SRR (a) by Au layer and (b) by Ag layer, respectively

reflection type PMC device was built on the p-type conductive silicon (Si) {100} substrate. The transmission type PMC devices were constructed on the fused silica ( $\text{SiO}_2$  glass), whose on both sides of them were optically polished to maintain the transparency before PMC fabrication. These substrates material were selected to design the PMC gate photo detector device, PMC optical waveguide or PMC non-linear optical devices, respectively. This time, we aimed to develop the fabrication process of PMC and the estimation of the fundamental properties of fabricated PMC structure with such substrates as the background dielectric material.

We constructed PMC structure on these substrates by two types of methods. One method was dry etching based and another one was based on lift off method, fundamentally. We briefly summarize the both methods as in follows.

As for the dry etching-based method, metallic layer or alternative stacking layers in several periods of metallic layers and dielectric material, such as  $\text{SiO}_2$  layers were evaporated on the substrate by RF sputtering method. The negative tone EB resist (such as NEB22 produced by Sumitomo Chemical Co. Ltd.) were spinning-coated and SRR array-based PMC pattern was exposure by electron beam lithography equipment (EBL7500-EX produced by ELIONIX INC. with 50 kV acceleration voltage). The patterned EB resist was used as the etching mask to fabricate metallic SRR structures by a dry etching process with reactive ion etcher (RIE) equipment. The dielectric over coating was applied in some cases to bury the SRR structure between dielectric layers.

The lift off-based fabrication process of PMC was as follows. The positive tone EB resist (for instance, ZEP-520A produced by ZEON Co.) was coated by spinning coater on

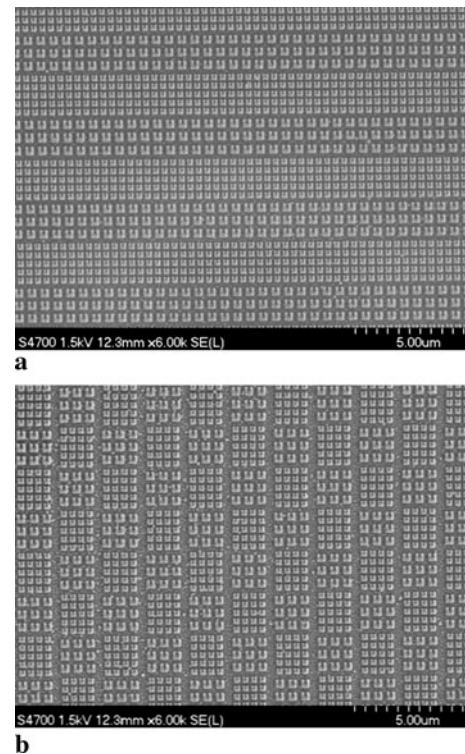


**Fig. 5** SEM images of (a) 1D and (b) 2D PMC structures

the substrate. EB lithography process was performed and lift off resist mask pattern was made. A metallic layer or the alternating stacking layers of metallic layers such as Au or Ag and dielectric layers such as  $\text{SiO}_2$  were evaporated on the sample top surface by RF sputtering apparatus. The lift off process was performed in the ultrasonic heating bath at suitable organic solvent temperature. A post dielectric capping is available, if it is necessary.

With these processes, we fabricated the 1D-PMC structure and 2D-PMC structure on the each substrate material. Scanning electron microscope (SEM) image of these structure with the dry etching method are listed shown in Figs. 5(a) and (b), respectively.

SEM-EDS elements mapping analysis results are shown in Figs. 6(a) and (b). Figure 6(a) shows the Au atomic element mapping and (b) for Ag atomic element mapping in different PMC samples.

These SEM-EDS mapping data showed that SRR structures were made by Au or Ag metallic layer successfully.

### 3.2 Optical and other properties of PMC structures

We show the mainly optical properties of the PMC structure samples, which have different SRR sizes but same in lattice constant of PMC structure. These samples were fabricated on silica substrate. Fraunhofer diffraction measurement with monochromatic laser beam and atomic probe microscope (AFM) measurement were performed on the PMC samples

to evaluate the physical dimension of the PMC lattice constant and so on. The reflection and transmission measure-

ments were performed on the samples to measure the reflection and transmission spectra for Ex and Ey polarized light. Also Raman mapping analysis was performed on the PMC samples fabricated on Si substrate.

### 3.2.1 Optical microscope images

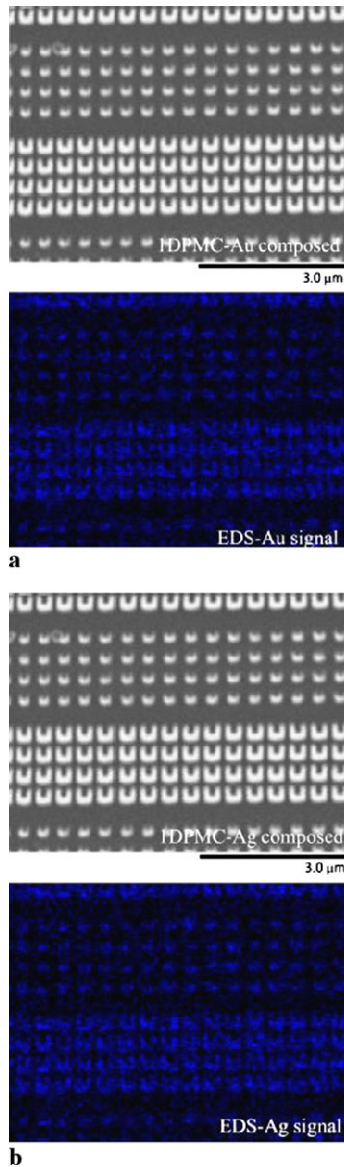
The PMC samples optical microscope images are shown in Fig. 7. The reason why we observe using an optical microscope images is to indicate that the pattern is formed in a wide area. Figures 7(a), (b), and (c) are for  $(L_1, L_2) = (160 \text{ nm}, 200 \text{ nm})$ ,  $(L_1, L_2) = (200 \text{ nm}, 220 \text{ nm})$  and  $(L_1, L_2) = (200 \text{ nm}, 300 \text{ nm})$ , respectively.  $(L_1, L_2)$  means the combination SRR with  $L = L_1$  and SRR with  $L = L_2$ . If there is a difference in LC resonance wavelength, the contrast is a good result. SRR structure is made by Ag in these samples. The substrate material was fused silica. Lift off method was used for these samples. Two Ag SRR arrayed layers has separated by a  $\text{SiO}_2$  RF sputtering layer.

### 3.2.2 AFM

AFM measurement results are shown in Fig. 8. Several defects of SRR structure can be seen in the PMC structure, but these defects might cause the broadening of SRR LC-resonance properties and PMC dispersion properties, but might be affected seriously as regards the PMC performance.

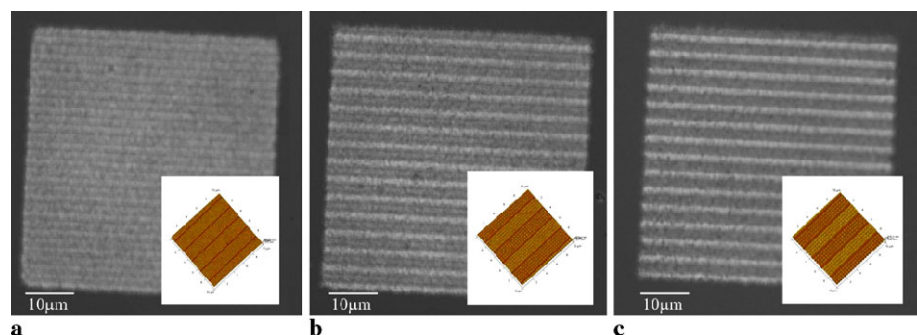
### 3.2.3 Fraunhofer diffraction

Horizontal Fraunhofer measurement results are shown in Fig. 9. We used a He-Ne laser (632.8 nm) for the monochromatic angular diffraction pattern measurement. The incidence angle is fixed at 60 degree to the substrate top surface normal. Si-photo detector with narrow slit was scanned in horizontal incidence plane around samples surfaces with step motion stage. From these safelight diffraction peaks, we obtained the PMC lattice constant as  $3.8 \mu\text{m}$ , in good agreement with AFM data and also the designed lattice constant.



**Fig. 6** SEM-EDS element mapping image of SRR structures composed (a) by Au layer and (b) by Ag layer, respectively

**Fig. 7** Optical microscope images of PMC samples (a), (b), and (c) are for  $(L_1, L_2) = (160 \text{ nm}, 200 \text{ nm})$ ,  $(L_1, L_2) = (200 \text{ nm}, 220 \text{ nm})$  and  $(L_1, L_2) = (200 \text{ nm}, 300 \text{ nm})$ , respectively





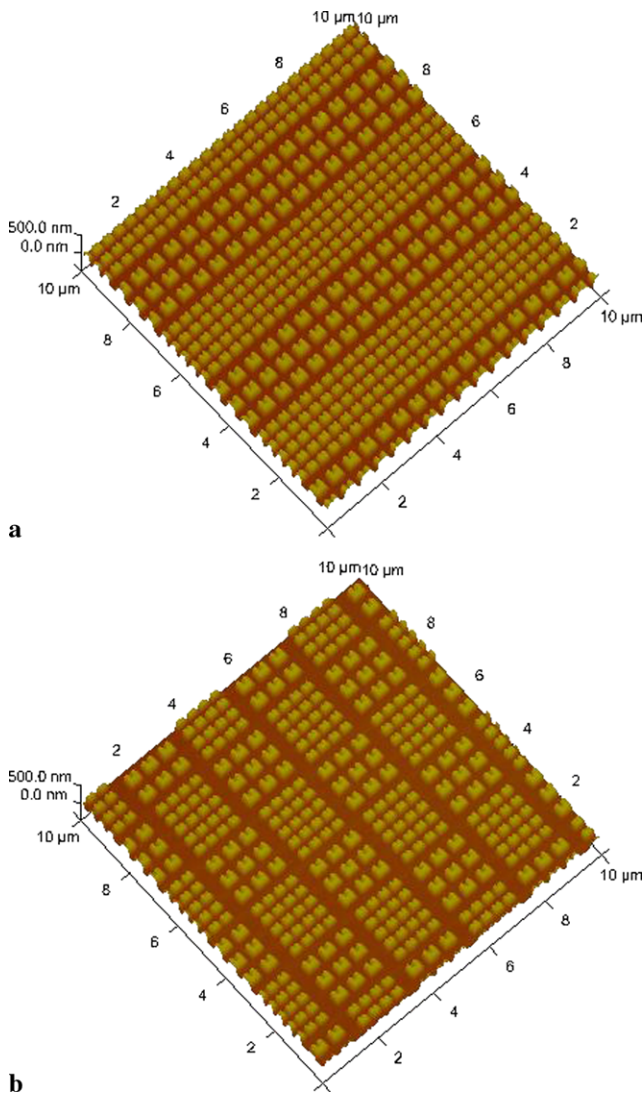


**Fig. 8** AFM topographic images of (a) 1D and (b) 2D PMC structures

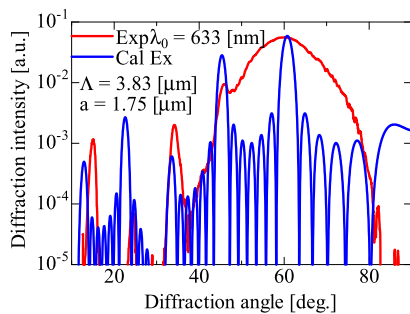


**Fig. 9** Fraunhofer diffraction measurement result

### 3.2.4 Reflection and transmission measurement

We show the reflection spectra of PMC for  $E_x$  and  $E_y$  polarization light in Fig. 10.

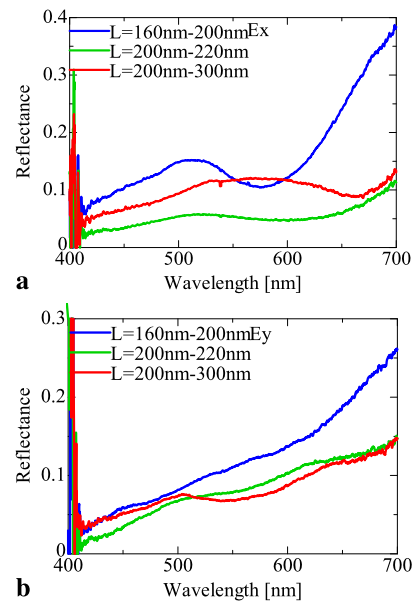


**Fig. 10** Reflection spectra for (a)  $E_x$  polarization and (b)  $E_y$  polarization

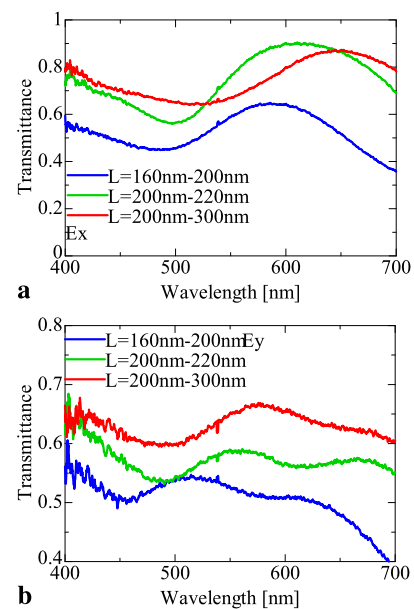


**Fig. 11** Transmission spectra for (a)  $E_x$  polarization and (b)  $E_y$  polarization

The transmission spectra for  $E_x$  and  $E_y$  polarization light are shown in Fig. 11.

### 3.2.5 Raman measurement

Raman scattering measurement was performed on PMC structure to check the nonlinear performance of the PMC structure. To estimate the selective resonant Raman properties on PMC structure, we performed laser Raman measurement with 532 nm DPSS light source. The 1D-PMC sample

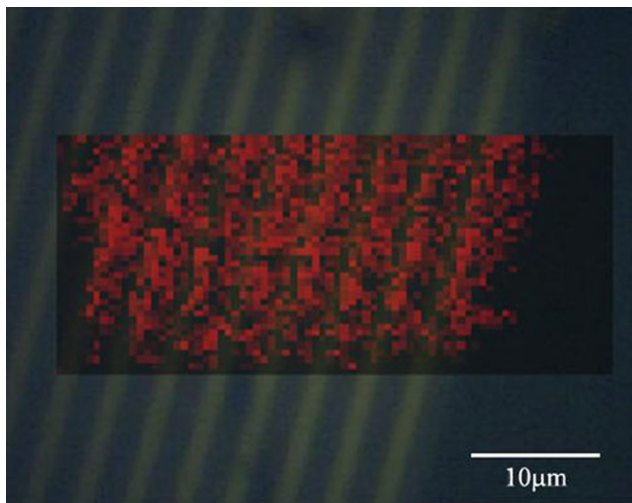


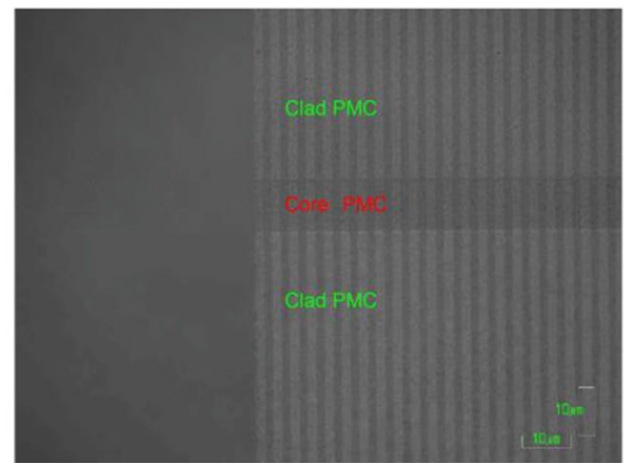
**Fig. 12** Selective resonant Raman effect in 1D-PMC structure ( $L_1, L_2$ ) = (200 nm, 300 nm)

on the Si substrate was used. A Raman intensity mapping at  $520 \text{ cm}^{-1}$  phonon peak was used to create the intensity map as shown in Fig. 12. From this picture, the areas whose SRR structure was smaller (having relatively higher resonance frequency) than non-excited area in 1D-PMC structure were resonantly excited by incident 532 nm excitation laser. These selective excitation properties can be caused by the optical field enhancement effect as shown in Fig. 4 by higher order LC-resonance at SRR structures.

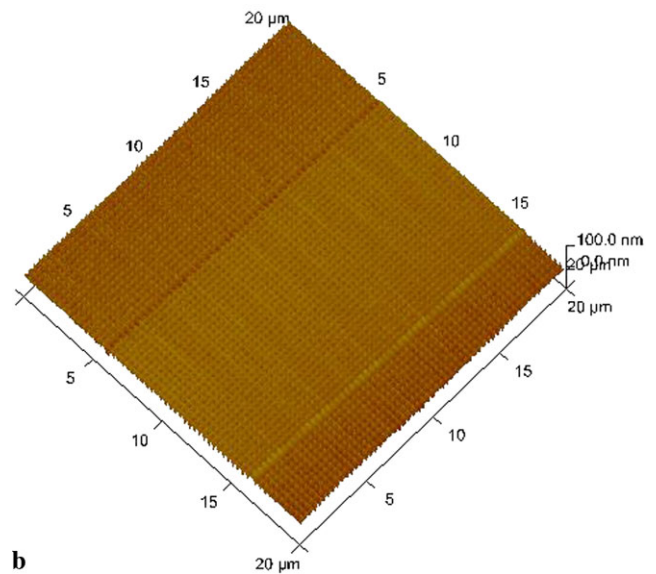
### 3.3 Fabrication of PMC waveguide structure

SRR-based PMC structures were used in waveguide as the core and clad layer to add specific the resonance dispersion properties to the waveguide. In such a structure, intentionally designed LC resonance mechanism cause the expected negative index property, we can design the optical confinement and dispersion of the waveguide by tuning the refractive index signs and absolute value and profiles. These tunings can be directly done by selecting the dielectric material working as the background dielectric material, structure, SRR size, sheet density, arraying ordering and so forth.

An example of PMC waveguide structure whose core and clad were composed by the PMC structures with different resonant frequency in each area is shown in Fig. 13. The SRR structure can be easily modified as regards the resonant properties by changing the SRR size. If the SRR resonant frequency is higher in the cladding than in the core, then it works as a waveguide at the relatively lower frequency and is leaky at the higher frequency compared to the average resonant frequency of core and clad. If the SRR resonant frequency is lower in the cladding than in core than in clad, it works as a waveguide at the relatively higher frequency and is leaky at the lower frequency compared to the average



**a**



**b**

**Fig. 13** PMC waveguide (a) is optical microscope image and (b) is AFM topographic image

frequency of the resonant frequency in core and that of the clad. This is just an example of the specific properties of PMC waveguide, but quite interesting for us as a potential application of the metamaterial.

## 4 Conclusions

We fabricated the photonic metamaterial crystal (PMC) surface structures and device, and obtained certain linear and nonlinear resonant properties. As an application field of metamaterial, we proposed a PMC waveguide and fabricated it in 2D-surface structure. These developments are just started and many unknown things exist, but PMC should be a promising material in future technologies.

**Acknowledgements** We thank Mr. Kurata, Mr. Ueki and Mr. Sugano for technical help in SEM investigations. The metallic layers dielectric properties estimation was performed under the auspices of Prof.

M. Fukui, and we are deeply grateful to him for his instructions on ATR measurement and surface Plasmon Polariton.

**Open Access** This article is distributed under the terms of the Creative Commons Attribution License which permits any use, distribution, and reproduction in any medium, provided the original author(s) and the source are credited.

## References

1. V.G. Veselago, *Sov. Phys. Usp.* **10**, 509 (1968)
2. V.G. Veselago, L. Braginsky, V. Shklover, C. Hafner, *Theor. Nanosci.* **3**, 189 (2006)
3. V.G. Veselago, E. Narimanov, *Nat. Mater.* **5**, 759 (2006)
4. J.B. Pendry, *Contemp. Phys.* **45**, 191 (2004)
5. C. Enkrich, M. Wegener, S. Linden, S. Burger, L. Zschiedrich, F. Schmidt, J. Zhou, T. Koschny, C.M. Soukoulis, *Phys. Rev. Lett.* **95**, 203901 (2005)
6. V.M. Shalaev, *Nat. Photonics* **1**, 41–48 (2007)
7. N. Liu et al., *Nat. Mater.* **7**, 31–37 (2008)
8. T. Okamoto, T. Fukuta, S. Satou, M. Haraguchi, M. Fukui, *Opt. Express* **19**(8), 7068–7076 (2011)
9. Photonics Global Conference 2012, vol. c12a512, Singapore, Dec. (2012)
10. S. Tretyakov, *Metamaterials* **1**, 40 (2007)
11. T. Okamoto, T. Otsuka, S. Sato, T. Fukuta, M. Haraguchi, *Opt. Express* **20**(21), 59–67 (2012)
12. M. Fukui, K. Matsugi, *J. Phys. Soc. Jpn.* **56**(8)
13. M. Haraguchi, M. Fukui, S. Muto, *Phys. Rev. B* **41**(2), 1254–1257 (1990)
14. E. Kretschmann, *Z. Phys. B* **241**, 313 (1971)
15. P. Drude, *Ann. Phys.* **1**, 566 (1900)